Desalination and Water Treatment
www.deswater.com

doi: 10.5004/dwt.2021.27101

222 (2021) 354–365
May

Application of Fe_3O_4@activated carbon magnetic nanoparticles for the adsorption of metronidazole from wastewater: optimization, kinetics, thermodynamics and equilibrium studies

Amir Sheikhmohammadi*, Esrafil Asgari*, Jaber Yeganeh

Department of Environmental Health Engineering, School of Health, Khoy University of Medical Sciences, Khoy, Iran, Postal number: 85167-53646, Tel. +98 04436252777; Fax: +98 04436257668; emails: a_sheikhmohammadi@khoyums.ac.ir/ asheikh1359@gmail.com (A. Sheikhmohammadi), esrafil_asgari@khoyums.ac.ir/sasgary@gmail.com (E. Asgari), jaber.yeganeh2@gmail.com (J. Yeganeh)

Received 25 May 2020; Accepted 31 January 2021

ABSTRACT

This study was conducted to investigate the application of activated carbon magnetic nanoparticles (AC-MNPs) as an adsorbent to remove metronidazole (MTZ) from aqueous solutions. Response surface methodology (RSM) using R software was employed to investigate the influence of operating parameters on the performance of AC-MNPs in the removal of MTZ. The obtained experimental data for AC-MNPs were tested with three RSM models. According to the obtained results of ANOVA, experimental data agreed with second-order model. The maximum removal efficiency (100%) was obtained under selected conditions (pH, 3.0; AC-MNPs dosage, 1.05 g/L; contact time, 90 min; MTZ concentration, 10 mg/L). The Freundlich isotherm and the pseudo-second-order kinetic models indicated reasonable correlation with the experimental data. The maximum adsorption capacity was 95.06 mg/g. Thermodynamic studies identified that MTZ adsorption onto AC-MNPs is spontaneous and endothermic. AC-MNPs show easy regeneration and good potential reusability, and its adsorption efficiency was preserved effectively even after five successive cycles of use. Therefore, AC-MNPs could be considered as an excellent adsorbent in the treatment of antibiotics and other organic pollutants.

Keywords: Adsorption; Fe_3O_4@activated carbon; Metronidazole; Modeling; Optimization

1. Introduction

In recent years, presence of antibiotics in the effluent of water and wastewater plants has received much attention [1]. This problem can affect the environment, ecosystem and quality of public health [1]. Antibiotics can cause irreversible long-lasting changes in the genome of microorganisms, making them resistant even to low concentrations [2]. Negative effects of antibiotics on human and animal reproductive system also have been reported [3]. Metronidazole (MTZ) with the chemical formula of $C_6H_9N_3O_3$ is one of the most commonly used antibiotics, which has anti-inflammatory and antibacterial properties [4]. This antibiotic is classified as a nitroimidazole and is used in the treatment of infectious diseases caused by anaerobic bacteria and protozoa. Low degradability, high solubility in water and accumulation in the environment are three characteristics of MTZ, which cause the removal of this antibiotic difficult from water by ordinary methods and sometimes impossible [2]. Therefore, according to the properties of MTZ and its adverse effects, it is necessary to control and remove this contaminant before it enters into water resources [5]. There are various alternatives to eliminate the medicinal compounds from aqueous environment.

* Corresponding authors.

These methods are adsorption [6], bioadsorption [7], membrane filtration (reverse osmosis or ultrafiltration) [8], advanced oxidation processes based on ozone [9], Fenton and photo-Fenton [5], irradiation (such as ultraviolet light or ultrasound) [10], photocatalysis using nanomaterials or advanced oxidation hybrid processes (such as O_3/UV/TiO_2 and O_3/H_2O_2) [4,11,12]. However, these methods have disadvantages that limit their application. Adsorption can be very effective even at very low concentrations (less than 1.0 mg/L of contaminant) [13]. In the removal of organic contaminants from water and wastewater, activated carbon (AC) has been widely used [7]. Activated carbon has high adsorption capacity and porosity for the removal of the specific organic matter such as antibiotics [14]. However, the application of powder adsorbents such as powdered activated carbon (PAC), due to difficulties encountered in separation and regeneration processes, has been limited. In the most previous studies, adsorbent separation was performed using filtration, centrifugation, decantation and precipitation methods [1,15]. Recently, magnetic separation method, due to its low cost, simplicity, fast separation and high performance has been widely used [16]. A saturated adsorbent is easily separated from aqueous solutions using a magnet. In this regard, various adsorbents such as zeolites, activated carbon fibers, ion exchange resins and even nanoparticles have been magnetized. Here, activated carbon magnetic nanoparticles (AC-MNPs), which combine the adsorption features of PAC with the excellent catalytic properties of Fe_3O_4 nanoparticles, were fabricated by a chemical co-precipitation technique. Studies related to adsorption of the antibiotics over the activated carbon have been reported very little in the literature [1]. The use of optimization techniques to improve process efficiency and minimize operational costs and time is quite essential. The classical optimization method (changing one factor and fixing others) due to lack of depicting the interactive effects of all the involved factors cannot be a precise and reliable method as expected. The response surface methodology (RSM) using R software can be a way to solve this problem. Because this method has the benefits of reduced operational costs, time and also includes the effect of all the factors involved in the adsorption process simultaneously. Therefore, the multivariable model (RSM) using the R software was applied to evaluate the AC-MNPs performance to remove MTZ from aqueous solutions.

2. Materials and methods

2.1. Materials and devices

All chemicals and reagents, including iron(III) chloridehexahydrate ($FeCl_3 \cdot 6H_2O$), iron(II) chloride ($FeCl_2 \cdot 4H_2O$), MTZ ($C_6H_9N_3O_3$, 98%), nitric acid (HNO_3, 1.0 N), ammonia (NH_3, 25%), and activated carbon powder were of analytical grade and were purchased from Merck Co. (Germany). Deionized water was used during the experiments. High performance liquid chromatography (Cecil 4100 Power stream Interface, England and operated with mobile phase of acetonitrile and distilled water (volume ratio 30:70) and a flow rate of 1.0 mL min^{-1}) was used to determine MTZ concentration in the solution. The pH was measured using Metrohm pH meter (model-827, Swiss). Shaker incubator (n-BioTEK NB-205) was used for mixing of solution. A magnet (1.3 Tesla) was used to isolate activated carbon magnetic nanoparticles.

2.2. Preparation of magnetic activated carbon

The chemical co-precipitation technique of Fe^{2+} and Fe^{3+} ions in the presence of activated carbon powder was applied to synthesize the AC-MNPs. For this purpose, 2.0 mL of nitric acid solution was mixed with 98 mL distilled water; then 10 g of activated carbon powder (incubated for 30 min) was gradually added to the solution. Then, the adsorbent was washed several times with distilled water to neutralize the acidic state and then was dried in the oven at 80°C for 24 h. In order to ensure the dispersion of activated carbon, the solution was sonicated for 20 min by sonication. Finally, in order to put iron oxide nanoparticles on activated carbon, 8.0 g of $FeCl_3$ and 2.5 g of $FeCl_2$ were added to the previous mixture. The mixture was placed on a heater. 50 mL ammonia (25%) was gently added and the mixture was re-mixed by ultrasound in the presence of nitrogen gas at the temperature above 70°C (200 rpm) for 2.0 h. At the end of the addition phase, the mixture temperature was raised to 90°C and stirred for 1 h. After completion, the resulting mixture was de-oxygenated four times with distilled water and washed once with ethanol. After neutralization of pH, the supernatant was removed and the residue was placed in the oven at 70°C for 5.0 h. Finally, after powdering and crystallizing of the nanoparticles in the presence of magnetic field, they were placed in a desiccator for dehumidification.

2.3. Magnetic activated carbon characterization

X-ray diffraction (XRD) patterns of AC-MNPs were collected by XRD measurement (Bruker, D8 Advance, Germany), with a radiation-producing copper anode (Cu-Kα) at 40 kV, 30 mA and 25°C. The scanning electron microscopy (SEM) at 15 keV was applied to investigate the surface morphologies of AC-MNPs. The shape and size of AC-MNPs were studied by transmission electron microscopy (TEM) at 100 keV. Brunauer–Emmett–Teller (BET) analysis, surface area, pore volume and pore size of Fe_3O_4, activated carbon and AC-MNPs were performed by Pore Size Determination (BJH) resorption method in N_2 medium at 77°K on autosorb surface area analyzer (Autosorb, Quanta Chrome Crop). The nanoparticles were degassed at 200°C under vacuum for 24 h (to remove the moisture). The magnetic properties of adsorbent were determined by vibrating sample magnetometer (VSM) method and with a VSM (MDKFD, Iran).

2.4. Adsorption experiments

Stock solution of MTZ was prepared by dissolving MTZ (10 mg) in methanol and deionized water; then transferred into a volumetric flask (100 mL). The solution was kept in the refrigerator until use. The desired concentrations of MTZ were prepared from this stock solution. Before each experiment, the solution pH was adjusted by the use of H_2SO_4 or NaOH (0.1 M). There are many variables that affect MTZ adsorption, including solution pH (3.0–11),

the AC-MNPs dosage (0.1–2.0 g/L), the contact time (5.0–90 min), and initial MTZ concentration (10–100 mg/L). Eqs. (1) and (2) calculated the amount of MTZ removal and the amount of MTZ uptake (q_e) at the equilibrium concentration was obtained, respectively [2]:

$$\text{Removal}\left(\%\right)=\frac{C_0-C_e}{C_0}\times 100 \tag{1}$$

$$q_e=\frac{\left(C_0-C_e\right)\times V}{W} \tag{2}$$

where C_0 and C_e are initial C_e and final MTZ concentration (mg/L), respectively. V and W are the volume of the solution (L) and the mass of the AC-MNPs (g), respectively.

2.5. Factorial experimental design

The RSM using CCD (the R software was used for this purpose) was applied as a useful statistical tool to consider the interaction effect of independent factors and dependent response. The CCD in the R software is an orthogonal design consisting of a factorial two-level design (with 2k points that form the base design) to which is added a 'star' design (axial points) with 2k points plus centre points, where k is the number of variables. Four parameters were considered in this study; therefore, the design of runs was done with involving these variables (Tables 1 and 2). After the design of runs, data coding was done and data were fitted with three models including first-order model (FO), first model with interaction (FI) and second-order (SO) model. The best model was selected according to ANOVA analysis (the lower p-value, higher F-value, higher R^2 and insignificant lack of fit). Then the final equation in terms of the coded factors was obtained by regression analysis of the selected model. After that, optimization process was done using the obtained formula and its results are presented in Table 2. Finally, contour plots were designed with involving two-way interaction response obtained by regression analysis of selected model.

3. Results and discussion

3.1. Magnetic activated carbon characterization

XRD analysis was used to identify the constituent phases and the structure of the AC-MNPs and the results are shown in Fig. 1.

For the activated carbon (AC), the broad peak at 2θ= 22° can be assigned to the characteristic reflection of carbon amorphous nature. As is evident, the Fe_3O_4 XRD patterns included five distinctive peaks at 2θ of 30.2°, 35.7°, 43.3°, 53.9°, and 63.2°, which correlate with the (220), (311), (400), (511), and (440) crystal planes, respectively. These XRD peak positions were in accordance with the standard pattern (JCPDS No. 19-0629), indicating pure iron oxide magnetite with inverted spinal cube structure [17]. In addition, all of the peaks were observed in AC-MNPs (Fig. 1). This indicates that the method of making magnetic activated carbon has not changed the crystal structure of iron oxide nanoparticles. The approximate mean size of the nanoparticles was calculated by placing the peak data of the AC-MNPs phase synthesized in Scherrer formula Eq. (3).

$$D=\frac{K\lambda}{\beta\cos\theta} \tag{3}$$

where the mean size of the nano-absorbent is (D), the constant number is equal to 0.89 (K), the wavelength of Cu-kα radiation is (λ = 1.54 Å), the main peak width is half of its intensity (in radians) (β) and the main peak position is in degrees (θ).

In this study, the size of magnetic activated carbon nanoparticles synthesized in the main peak at position 2θ ~ 35.7° was 52.3. Shape, size and morphology of particles were determined by SEM. Analysis of SEM (Fig. 2) proved the presence of Fe_3O_4 nanoparticles with spherical nanoscale structures (in the range of 36.2–49.5 nm; Fig. 2a) and AC-MNPs with less agglomerated surface and structure of non-uniform (in the range of 40.2–55.5 nm; Fig. 2b). According to TEM image (Fig. 3), Fe_3O_4 nanoparticles have a cubic structure and relatively distributed in a uniform way on the surface of AC. Also based on TEM results, size of AC-MNPs was estimated to 20–35 nm that was consistent with XRD analysis.

The magnetic effect of the magnetically synthesized activated carbon and Fe_3O_4 nanoparticles is shown in Fig. 4. The magnetization of AC-MNPs was 24.93 emu/g, which showed a reduction in magnetization compared with 46.65 emu/g for Fe_3O_4 nanoparticles. This reduction is probably due to the coating created and the magnetic effects of the coating reduced. Finally, the results of magnetometry test show confirmation of para-magnetic property of the synthesized AC-MNPs.

Table 3 depicts BET analysis, surface area, pore volume and pore size of Fe_3O_4, activated carbon and AC-MNPs. The results illustrated that the AC-MNPs composite, with an average diameter of 42.67 nm, falls into the mesopore category, according to IUPAC classification of pore size (Mesopore [2 < d < 50 nm]) [18]. Also, it is found that AC has a very small surface area (8.0 m²/g) with pore volume (0.0057 cm³/g) and Fe_3O_4 nanoparticles have a surface area (85 m²/g) with pore volume (0.035 cm³/g; Table 3). Subsequently, the surface area of synthesized magnetic activated carbon nanoparticles increased (60 m²/g) with pore volume (0.0297 cm³/g), which increased the ability to adsorb pollutants.

3.2. Results in the response surface model

The obtained data from experiments were fitted with three RSM models (FO, FI and SO). Table 4 presents comparison of the different RSM models. According to Table 4, the FO, FI models indicated significant lack of fit, whereas the value of lack of fit for SO model was insignificant. Given that, value of the lack of fit must be insignificant in a well-fitted model; the FO and FI models (due to significant lack of fit) did not indicated the satisfactory agreement with the experimental data. According to ANOVA analysis (Table 5), SO model due to the lower p-value, higher

Table 1
Actual and coded values of independent variables used for experimental design

Variable	Symbol	Coded level (AC-MNPs)		
		–1	0	+1
		Real values		
Metronidazole concentration (mg/L)	X_1	10	55	100
AC-MNPs dose (g/L)	X_2	0.1	1.05	2
Time (min)	X_3	5	47.5	90
pH	X_4	3	7	11

AC MNPs: activated carbon magnetic nanoparticles.

Table 2
Central composite design matrix with uncoded values of the variables

Sl. no.	Uncoded values					% Removal		
	X_1	X_2	X_3	X_4	Expt. (γ)	Pred. (γ)		
						Lower	Fit	Upper
1	10	0.1	5	3	28	27.53813	21.22505	33.85122
2	10	1.05	5	7	35.02	36.22411	30.01854	42.42968
3	55	1.05	47.5	7	60.2	59.32857	54.36798	64.28917
4	55	1.05	47.5	7	61.3	59.32857	54.36798	64.28917
5	10	0.1	47.5	3	64.5	64.82168	59.09274	70.55061
6	10	2	47.5	3	93.5	96.55501	90.82607	100
7	10	2	90	3	100	98.77352	92.40322	100
8	10	1.05	90	7	80.08	78.87589	72.67032	85.08146
9	55	1.05	47.5	7	58.2	59.32857	54.36798	64.28917
10	55	1.05	47.5	7	59.3	59.32857	54.36798	64.28917
11	10	1.05	90	3	98	99.65569	94.06752	100
12	10	1.05	47.5	11	55	53.79589	47.59032	60.00146
13	55	1.05	47.5	7	62.3	59.32857	54.36798	64.28917
14	55	1.05	47.5	7	59.5	59.32857	54.36798	64.28917
15	10	1.05	90	11	63.01	64.21411	58.00854	70.41968
16	55	1.05	47.5	7	58.9	59.32857	54.36798	64.28917
17	10	0.1	90	3	77	77.14019	70.76989	83.51049
18	10	2	5	3	71.2	69.37147	63.05838	75.68455
19	10	1.05	90	3	97	99.65569	94.06752	100
20	55	1.05	90	3	86.02	88.48353	83.26826	93.69881
21	100	1.05	90	3	78	77.31138	71.08367	83.53908
22	55	1.05	5	3	34.12	35.20629	28.85722	41.55536
23	55	1.05	47.5	3	76.5	74.32743	68.66586	79.98900

F-value and higher R^2 than those of the FO and FI models indicated a satisfactory agreement with the experimental data. Therefore, this model (SO) was selected for prediction and optimization of experimental data. As shown in Table 5, SO model includes first-order response (X_1, X_2, X_3, X_4), two-way interaction response (X_1, X_2, X_3, X_4) and full second-order response (X_2, X_3, X_4). The final equation in terms of the coded factors was obtained by regression analysis of the selected model (Table 5). Also regression analysis of the SO model indicated that the terms of X_1, X_2, X_3, X_4, X_1: X_3, X_1: X_4, X_2: X_3, X_2^2 and X_3^2 have the important role in the adsorption process and can be included in the final equation (Table 6). Although, the influence of the terms (X_2, X_3, X_1: X_3, X_1: X_4) and (X_1, X_4, X_2: X_3, X_2^2, X_3^2) on the adsorption of MTZ

by AC-MNPs was synergic and antagonistic, respectively. According to regression analysis of the SO model, the final equation in terms of the coded factors can be written as follows (Eq. (4)):

$$Y = 59.32857 - 10.70394X_1 + 15.86667X_2 + 28.21348X_3 - 13.43232X_4 + 6.88759X_1{:}X_3 + 8.27528X_1{:}X_4 - 5.05\ X_2{:}X_3 - 11.69883X_2^2 - 12.48252X_3^2 \quad (4)$$

After that, optimization process was done using the obtained formula and results are presented in Table 2. As achieved results, the optimum predicted conditions (with considering the maximum removal efficiency (100 %)) for SO

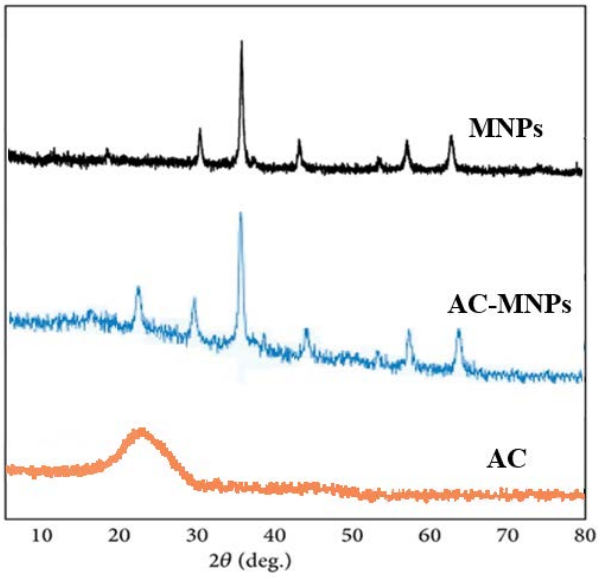

Fig. 1. X-ray diffraction analysis of activated carbon magnetic nanoparticles and its ingredients.

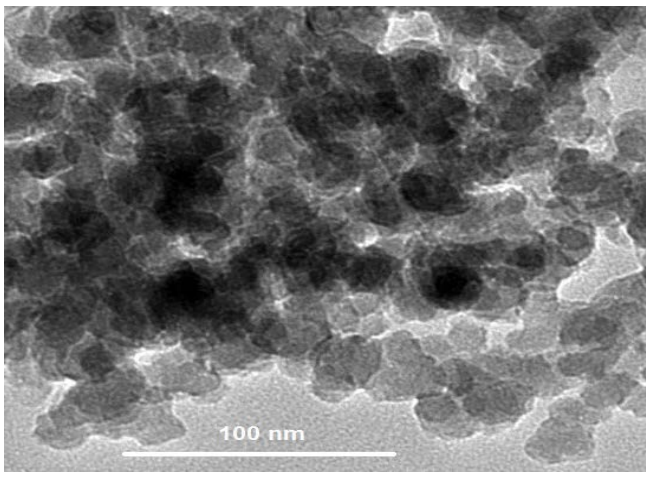

Fig. 3. Transmission electron microscopy images of activated carbon magnetic nanoparticles.

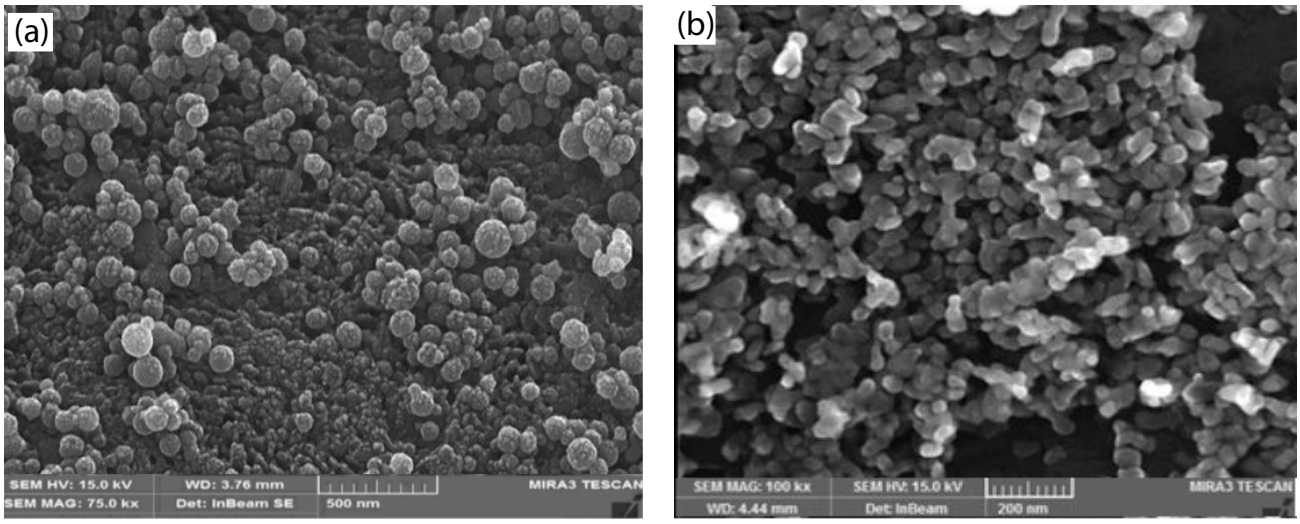

Fig. 2. Scanning electron microscopy images of (a) Fe_3O_4 nanoparticles and (b) activated carbon magnetic nanoparticles.

Table 3
BET analysis, surface area, pore volume and pore size of Fe_3O_4, AC and AC-MNPs

Material	Surface area (m^2/g)	Pore volume (cm^3/g)	Pore size (Å)
Fe_3O_4	85	0.035	4.242
AC	8.0	0.0057	4.021
AC MNPs	60	0.0297	4.267

AC: activated carbon; AC MNPs: activated carbon magnetic nanoparticles.

model were achieved at pH, 3.0; AC-MNPs dosage, 1.05 g/L; contact time, 90 min and MTZ concentration, 10 mg/L.

In the following, the model adequacy and reliability was also assessed using actual and predicted values. As observed in Fig. 5, it was confirmed that the predicted values are close to the actual values.

3.3. Description of 3D plots

The interactive effect is very critical in the adsorption of pollutant on the adsorbent. Fig. 6a revealed the interactive influence of reaction time and adsorbent mass on the removal performance of MTZ by AC-MNPs. It was observed at the constant time of 40 min, with increasing the adsorbent dosage from 0.5 to 2.0 g/L, the removal performance incremented and reached from 40% to 70%. Also at the constant AC-MNPs dosage, improvement in the performance was revealed with increasing the contact. This phenomenon can be related to availability of larger number of sorption sites to adsorb MTZ and also increase in adsorption capacities (as a higher amount of adsorbent was used). The increase of removal performance at the promoted contact time can be interpreted to that with increasing contact time; the chance of collision of pollutant with adsorbent is elevated, causing a direct effect on the adsorption performance.

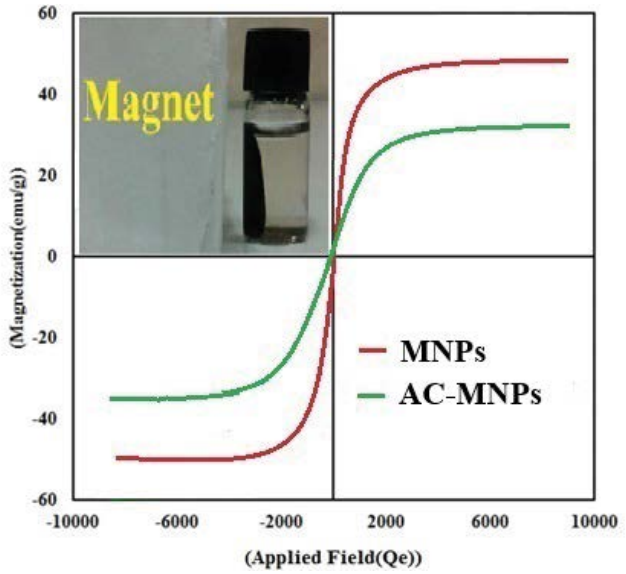

Fig. 4. Vibrating sample magnetometer images of activated carbon magnetic nanoparticles.

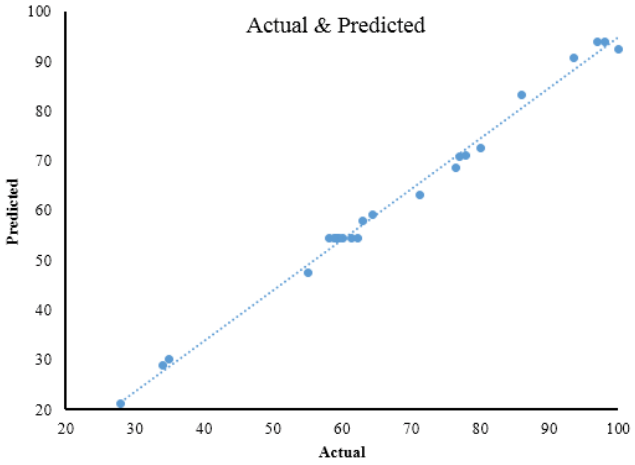

Fig. 5. Adequacy plots of the fitted model for the MTZ adsorption by activated carbon magnetic nanoparticles.

Table 4
Comparison of different models of RSM for fitting a response surface model

Models	Multiple *R*-squared	Adjusted *R*-squared	*F*-statistic	*p*-value	Lack of fit
FO	0.91	0.89	46.39 on 4 and 18 DF	3.044e-09	6.847e-05
FI	0.94	0.91	28.87 on 8 and 14 DF	2.049e-07	8.960e-05
SO	0.99	0.98	183.9 on 11 and 11 DF	8.036e-11	0.065

Table 5
Analysis of variance for the second-order model

Model formula in RSM	DF	Sum of squares	Mean square	*F*-value	Probability (*P*)
First-order response (X_1, X_2, X_3, X_4)	4	8,239.1	2,059.76	463.4218	3.549e-12
Two-way interaction response (X_1, X_2, X_3, X_4)	4	282.7	70.69	15.9035	0.0001521
Full second-order response (X_2, X_3, X_4)	3	467.6	155.88	35.0714	6.327e-06
Residuals	11	48.9	4.44	–	–
Lack of fit	4	33.0	8.25	3.6331	0.0658636
Pure error	7	15.9	2.27	–	–

Table 6
Regression analysis of the second-order model

	Uncoded values			
Model term	Coefficient estimate	Std. error	*t*-value	*p*-value
(Intercept)	59.32857	0.79684	74.4547	3.191e-16
X_1	–10.70394	2.18338	–4.9025	0.0004698
X_2	15.86667	0.86069	18.4349	1.279e-09
X_3	28.21348	1.83267	15.3947	8.668e-09
X_4	–13.43232	3.10358	–4.3280	0.0011985
X_1:X_3	6.88759	1.55644	4.4252	0.0010196
X_1:X_4	8.27528	3.07766	2.6888	0.0210736
X_2:X_3	–5.05000	1.05412	–4.7907	0.0005617
X_3:X_4	1.77171	1.53621	1.1533	0.2732317
X_2^2	–11.69883	1.99462	–5.8652	0.0001085
X_3^2	–12.48252	1.38197	–9.0324	2.024e-06
X_4^2	3.87157	2.52731	1.5319	0.1537892

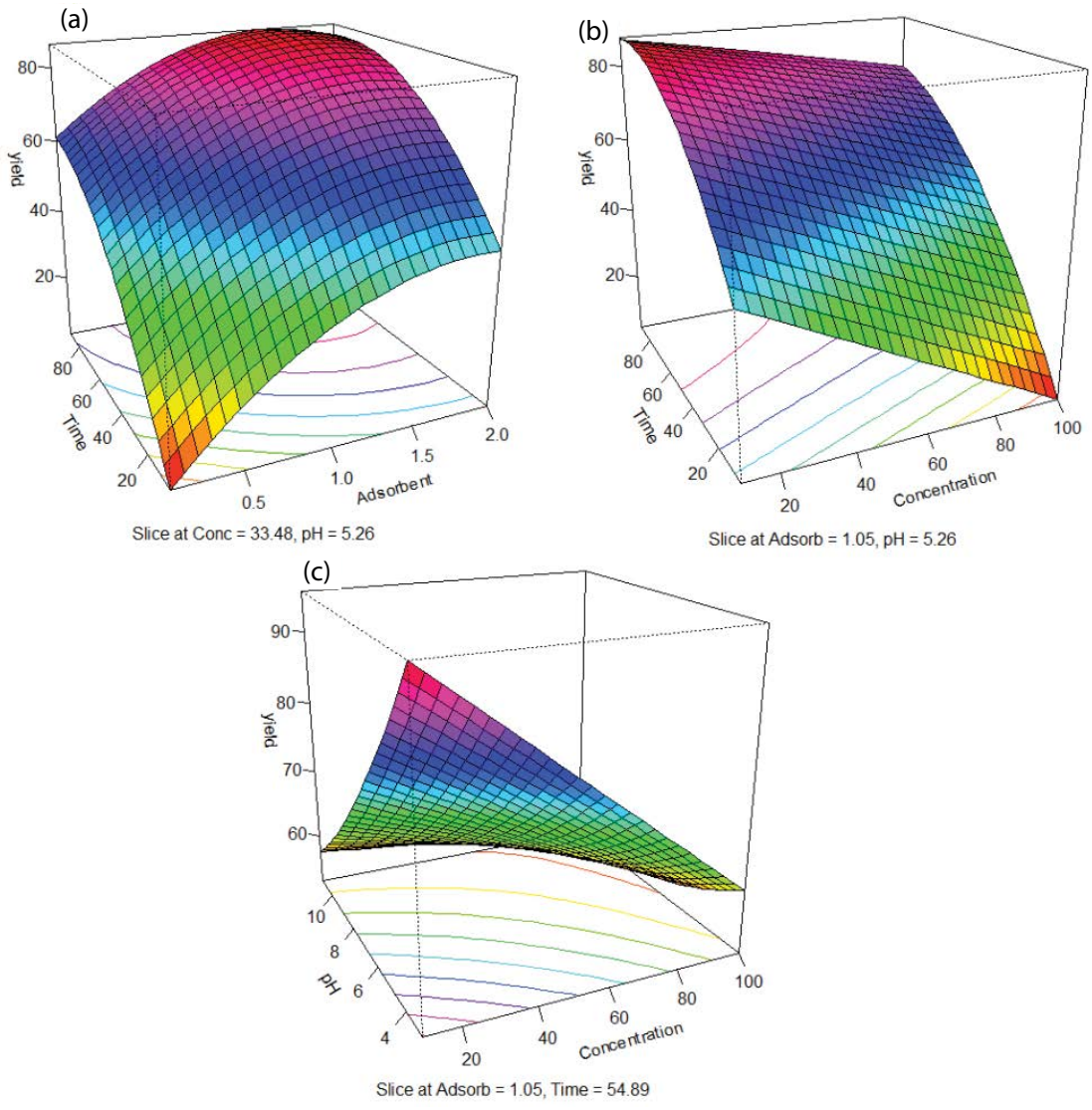

Fig. 6. 3D plots (a) time and adsorbent dosage, (b) time and MTZ concentration, (c) pH and initial MTZ concentration.

On the other hand, it is observed that the adsorption rate at early contact times is higher, which could be assigned to further availability to surfaces and pores of the adsorbent at early contact times, and lower availability to that at higher contact times due to occupancy of the surface with the pollutant [19]. As Fig. 6b shows, increase in the MTZ concentration (with fixing other factors) resulted in decrease of removal performance, whereas increase of contact time improved the MTZ removal rate. This manner can be due to decrease of the sorption capacity of AC-MNPs by increasing the MTZ concentration. Also reason of the MTZ removal improvement with increasing the contact time (at the fixed MTZ concentration) can be due to applying the internal parts of the adsorbent for MTZ sorption. In contrast, because of the increase of collision chance of the MTZ to the adsorbent surface in the higher MTZ concentration, the adsorption capacity is expected to increase. This occurrence can be explained in this way that with increasing initial concentration, the driving force for mass transfer is enhanced, causing the increase of the transfer velocity of MTZ molecules from the solution to the surface water layer surrounding the absorbent, and subsequent velocity increase of the transfer of MTZ molecules to the porous spaces of the adsorbent. Therefore, with increase of the MTZ concentration, the adsorption amount per mass unit of the AC-MNPs is elevated [19]. As Fig. 6c shows, at the constant concentration of MTZ (40 mg/L), with increasing pH from 4.0 to 10, removal performance was diminished from 80% and reached to 60%. Solution pH has the important role in controlling the reaction rate and can affect the adsorption process. The modification of the surface of AC by Fe_3O_4 nanoparticles can change the surface properties of AC and its zero point charge (pH_{zpc}). In AC-MNPs, zero point charge is 6.6 (Fig. 7). Accordingly, adsorbent surface is positively charged at pH < pH_{zpc} while it became negative at pH > pH_{zpc} [16]. Also, MTZ has electron-rich aromatic rings tending to be adsorbed on the positively charged surface of adsorbent. Considering the pK_a values of MTZ (pK_{a1} = 2.55) [20], it is assumed that ionic species of MTZ vary from neutral charge at acidic pH values to negative charge at neutral and alkaline pHs, which confirms the acceleration in the adsorption efficiency of MTZ. However, in the neutral and acidic pHs of the solution, there is not an electrostatic repulsing force, and the Van der Waals attraction, hydrophobic interaction and hydrogen bands can be suggested to be the main agents of increase in the removal performance. It worth noting that the MTZ molecules and OH^- at base pHs compete to each other to occupy the adsorbent surface, so that it might be affective in decreasing the removal performance [21]. Tang et al. [22] reported that adsorption of ciprofloxacin and norfloxacin on the reduced graphene oxide/magnetite composites (RGO-M) was strongly dependent on pH. Similar adsorption behaviors for MTZ and other antibiotics have been reported by other researchers [3,23].

3.4. Adsorption isotherms of MTZ onto AC-MNPs

Reaction description of pollutant with adsorbent was depicted by adsorption isotherms. For this purpose, two isotherm models including Langmuir and Freundlich were tested to survey the adsorption performance. Langmuir and Freundlich models are based on homogeneous (single-layer) and heterogeneous (multi-layer) adsorption, respectively. The linear forms of Langmuir and Freundlich models are expressed in Eqs. (5) and (6), respectively [24,25].

$$\frac{C_e}{q_e} = \frac{1}{k_f q_m} + \frac{C_e}{q_m} \tag{5}$$

$$\ln q_e = \ln k_f + \left(\frac{1}{n}\right) \ln C_e \tag{6}$$

where q_m (mg/g) is the maximum amount of adsorbed MTZ per mass unit of adsorbent, k_f (L/mg) is the Langmuir adsorption constant, C_e (mg/L) is the equilibrium concentration of MTZ in solution, k_f (mg/g (L/mg)$^{1/n}$) is the constant related to the adsorption intensity and n is the constant related to the adsorption capacity. The value of q_m (the maximum amount of MTZ adsorption onto AC-MNPs) was calculated to be 95.05 mg/g at 25°C (Table 7 and Fig. 8). It was revealed that the Freundlich isotherm model (R^2 > 0.98) and n > 1 (Table 7) can be an appropriate model than the Langmuir [18,26]. Therefore, it was proved that the adsorption of MTZ onto AC-MNPs can be multi-layer.

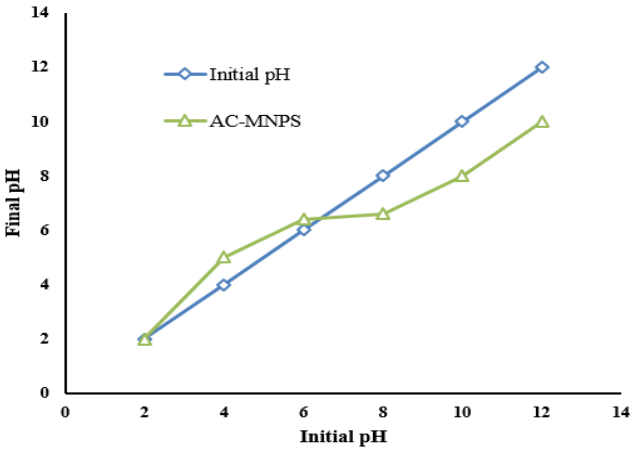

Fig. 7. pH_{zpc} of activated carbon magnetic nanoparticles.

Table 7
Isotherm parameters of MTZ adsorption onto of activated carbon magnetic nanoparticles

Isotherm equation	Isotherm parameters	Temperature (°C)		
		25	35	45
Langmuir	q_m (mg/g)	95.06	53.76	46.06
	k_f	0.25	0.28	0.35
	R_L	0.073	0.053	0.065
	R^2	0.927	0.935	0.958
Freundlich	n	2.66	2.57	2.38
	k_f (mg/g (L/mg)$^{1/n}$)	20.81	12.83	10.68
	R^2	0.982	0.992	0.995

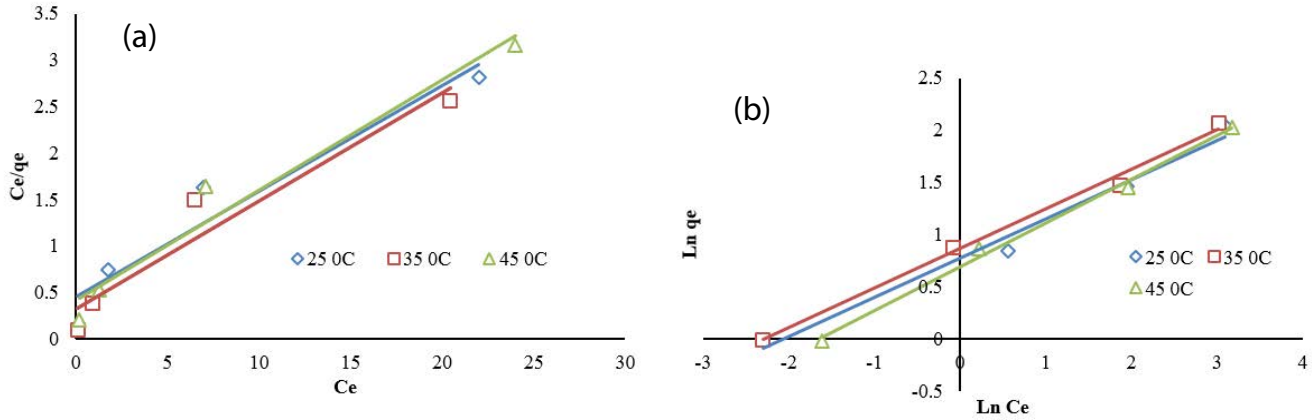

Fig. 8. Langmuir (a) and Freundlich (b) isotherms of MTZ adsorption onto of activated carbon magnetic nanoparticles.

3.5. Adsorption kinetics of MTZ onto AC-MNPs

The adsorption kinetics of MTZ onto AC-MNPs was analyzed by two kinetic models including pseudo-first-order and pseudo-second-order (Eqs. (7) and (8)) [27,28]:

Pseudo-first-order model:

$$\ln\left(q_e - q_t\right) = \ln q_e - k_e t \tag{7}$$

Pseudo-second-order model:

$$\frac{t}{q_t} = \frac{1}{k_f q_e^2} + \frac{t}{q_e} \tag{8}$$

where q_t (mg/g) is the MTZ absorbed at t time, q_e (mg/g) is the MTZ absorbed at the equilibrium time, k_e (1/min) is the constant of first-order absorption and k_f (g/(mg min)) is the constant of second-order absorption. It was revealed that pseudo-second-order model with R^2 values of above 0.99 at all initial MTZ concentrations (Table 8) can be appropriate model than the first-order model. In addition, with regard to the maximum regression coefficients, the pseudo-second-order model can be applied to determine the adsorption capacity (q_{cal}), which is consistent with the corresponding experimental value (q_{exp}). Consequently, the pseudo-second-order model is the appropriate model for describing MTZ adsorption onto the AC-MNPs. This suggests that the adsorption of MTZ on AC-MNPs is chemisorption in nature [29].

3.6. Thermodynamic study

Thermodynamic study of MTZ adsorption onto AC-MNPs was conducted according to Eqs. (9)–(11) [28] and results are presented in Table 9.

$$\Delta G° = -RT\left(\ln K_c\right) \tag{9}$$

$$\ln K_c = \frac{\Delta S°}{R} - \frac{\Delta H°}{RT} \tag{10}$$

$$K_c = \frac{q_e}{C_e} \tag{11}$$

where $\Delta G°$(kJ/mol) is the free energy change, T (K) is the solution temperature, R (J/mol/K) is the universal gas constant (8.314 J/mol/K), $\Delta H°$ (kJ/mol) is the standard enthalpy, $\Delta S°$ (J/mol/K) is the standard entropy and K_c (L/g) is the equilibrium constant of the adsorption. The values of negative $\Delta G°$, positive $\Delta H°$ and positive $\Delta S°$ indicated MTZ adsorption process onto AC-MNPs is spontaneous, endothermic, and increase the disorder at the liquid–solid interface with increasing temperature, respectively.

Table 8
Kinetic parameters of MTZ adsorption onto activated carbon magnetic nanoparticles

Kinetic model	Kinetic parameters	MTZ concentration (mg/L)			
		10	25	50	100
Pseudo-first-order	q_{exp} (mg/g)	82.04	45.32	23	10.2
	q_e (mg/g)	1.29	3.47	7.07	14.32
	k_e (1/min)	0.0033	0.0036	0.0039	0.0039
	R^2	0.883	0.722	0.742	0.7251
Pseudo-second-order	q_e (mg/g)	95	50	25.64	13.33
	k_f (g/(mg min)	0.21	0.071	0.027	0.011
	R^2	0.998	0.999	0.998	0.997

3.7. Comparison with literature results

The maximum AC-MNPs adsorption capacity (q_m) was compared with MTZ adsorption capacities for various reported adsorbents (Table 10). As tabulated in Table 10, the AC-MNPs had a higher adsorption capacity (95.06 mg/g) compared with other processes.

3.8. Recycling and regeneration of the adsorbent

The AC-MNPs were used for MTZ adsorption and recycled for five consecutive adsorption runs. According to Fig. 9, the MTZ removal percentage by AC-MNPs reduced from ~100% to 90.5% after five recycling cycles. In other words, the AC-MNPs could be adopted for the elimination of MTZ from aqueous solutions for five cycles if the removal efficiency above 90.5% is expected. Moreover, desorption by HCl was more efficient than desorption by NaOH in all adsorption–desorption runs. In the first and fifth desorption steps, the HCl desorption solution resulted in >82.2% and 50.3% MTZ desorption from the AC-MNPs, while the NaOH desorption solution gave 36% and 19.2% MTZ desorption, respectively. The high efficiency of HCl in desorbing MTZ from the AC-MNPs can be a consequence of AC-MNPs surface protonation by this acid.

Table 9
Thermodynamic parameters of MTZ adsorption onto activated carbon magnetic nanoparticles

Concentration (mg/L)	$\Delta G°$			$\Delta S°$	$\Delta H°$
	298°K	308°K	318°K		
10	–5.67992	–5.87052	–4.2017	499.2557	144.4059
25	–0.71533	–2.46386	–1.69697	106.3361	28.03481
50	1.203191	1.028449	1.316773	116.5623	32.60751
100	2.569041	2.416204	3.03873	61.5236	17.52591

Table 10
Maximum adsorption capacity of some adsorbents for antibiotics removal from aqueous solutions

Research number	Adsorbent (Antibiotic) types	Removal time	q_m (mg/g)	Reference
1	Activated carbon (Sulfamethazine)	12 h	3.07	[30]
2	Activated carbon modified by Fe^{3+} (Sulfamethazine)	12 h	17.24	[30]
3	Activated carbon (sulfamethoxazole)	290 min	95.96	[31]
4	Activated carbon (metronidazole)	150 min	77.66	[31]
5	MWCNTs (levofloxacin)	80 min	9.8	[32]
6	MWCNTs (metronidazole)	80 min	4.8	[32]
7	Concrete-containing graphene (metronidazole)	60 min	54.35	[33]
8	Powder activated carbon (metronidazole)	60 min	0.076	[33]
9	Activated carbon magnetic nanoparticles (metronidazole)	90 min	95.06	This work

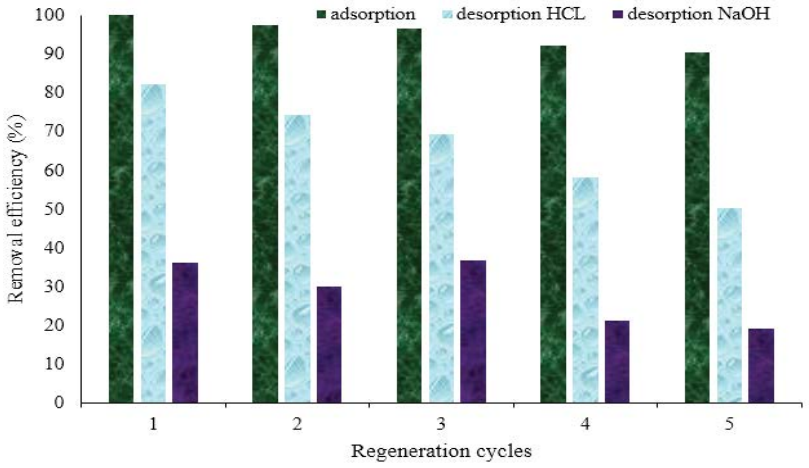

Fig. 9. Efficiency of fresh and regenerated activated carbon magnetic nanoparticles in the removal of MTZ. HCl and NaOH were used as the desorption solutions.

4. Conclusions

In the present study, Fe_3O_4@activated carbon (AC-MNPs) was synthesized and characterized as a composite to adsorb of MTZ from aqueous solutions. RSM-based modeling using R software was employed to investigate the influence of the operating parameters on the performance of AC-MNPs in the removal of MTZ. According to ANOVA analysis, SO model was selected as only appropriate model for prediction and optimization of experimental data. The maximum removal efficiency (100%) was obtained at pH, 3.0; AC-MNPs dosage, 1.05 g/L; contact time, 90 min and MTZ concentration, 10 mg/L). Results indicated that the adsorption of MTZ onto AC-MNPs follows the Freundlich isotherm, and the maximum adsorption capacity was obtained as approximately 95.06 mg/g. Thermodynamic studies identified endothermic nature of the adsorption process. Finally, it can be concluded that the AC-MNPs can be considered as promising adsorbent to be utilized in adsorption process of MTZ pollutants and similar compounds from aquatic environments.

Acknowledgment

The present study is the result of a project with ethical code: IR.KHOY.REC.1398.345. The authors would like to thank the Khoy University of Medical Sciences for all the supports provided.

Author contributions

A. SH (Senior Researcher) designed the experiments, collected the data and interpreted the experimental work. E.A. (Assistant Professor) did data compilation and jointly wrote the paper. J.Y. (Ph.D.) reviewed the whole work and provided suggestions for the improvement of the paper.

References

[1] D. Balarak, F.K. Mostafapour, H. Akbari, A. Joghtaei, Adsorption of amoxicillin antibiotic from pharmaceutical wastewater by activated carbon prepared from *Azolla filiculoides*, J. Pharm. Res. Int., 18 (2017) 1–13.
[2] A. Dehghan, A.A. Mohammadi, M. Yousefi, A.A. Najafpoor, M. Shams, S. Rezania, Enhanced kinetic removal of ciprofloxacin onto metal-organic frameworks by sonication, process optimization and metal leaching study, Nanomaterials, 9 (2019) 1422.
[3] S.D.K. Silva, S.D.M. Hasan, M.F. Rosa, degradation of the antibiotic metronidazole by advanced oxidative processes, Period. Tche Quim., 14 (2017) 72–86.
[4] E. Asgari, A. Esrafili, A.J. Jafari, R.R. Kalantary, M. Farzadkia, Synthesis of TiO_2/polyaniline photocatalytic nanocomposite and its effects on degradation of metronidazole in aqueous solutions under UV and visible light radiation, Desal. Water Treat., 161 (2019) 228–242.
[5] B. Kamarehie, F. Ahmadi, F. Hafezi, A. Abbariki, R. Heydari, M.A. Karami, Experimental data of electric coagulation and photo-electro-phenton process efficiency in the removal of metronidazole antibiotic from aqueous solution, Data Brief, 18 (2018) 96–101.
[6] D. Carrales-Alvarado, R. Ocampo-Pérez, R. Leyva-Ramos, J. Rivera-Utrilla, Removal of the antibiotic metronidazole by adsorption on various carbon materials from aqueous phase, J. Colloid Interface Sci., 436 (2014) 276–285.
[7] I. Nasseh, M. Khodadadi, R. Khosravi, A. Beirami, N. Nasseh, Metronidazole removal methods from aquatic media: a systematic, Ann Milit. Health Sci. Res., 14 (2016) e13756.
[8] D. Dolar, M. Gros, S. Rodriguez-Mozaz, J. Moreno, J. Comas, I. Rodriguez-Roda, D. Barceló, Removal of emerging contaminants from municipal wastewater with an integrated membrane system, MBR–RO, J. Hazard. Mater., 239–240 (2012) 64–69.
[9] F. Bahrami Asl, M. Kermani, M. Farzadkia, A. Esrafili, S. Salahshour Arian, D. Zeynalzadeh, Removal of metronidazole from aqueous solution using ozonation process, J. Mazandaran Univ. Med. Sci., 24 (2015) 131–140.
[10] Y. Deng, R. Zhao, Advanced oxidation processes (AOPs) in wastewater treatment, Curr. Pollut. Rep., 1 (2015) 167–176.
[11] S. Agarwal, I. Tyagi, V.K. Gupta, M. Sohrabi, S. Mohammadi, A.N. Golikand, A. Fakhri, Iron doped SnO_2/Co_3O_4 nanocomposites synthesized by sol-gel and precipitation method for metronidazole antibiotic degradation, Mater. Sci. Eng. C, 70 (2017) 178–183.
[12] J. Deng, M. Xu, S. Feng, C. Qiu, X. Li, J. Li, Iron-doped ordered mesoporous Co_3O_4 activation of peroxymonosulfate for ciprofloxacin degradation: performance, mechanism and degradation pathway, Sci. Total Environ., 658 (2019) 343–356.
[13] M.H. Dehghani, A. Zarei, A. Mesdaghinia, R. Nabizadeh, M. Alimohammadi, M. Afsharnia, Response surface modeling, isotherm, thermodynamic and optimization study of arsenic (V) removal from aqueous solutions using modified bentonite-chitosan (MBC), Korean J. Chem. Eng., 34 (2017) 757–767.
[14] E.K. Putra, R. Pranowo, J. Sunarso, N. Indraswati, S. Ismadji, Performance of activated carbon and bentonite for adsorption of amoxicillin from wastewater: mechanisms, isotherms and kinetics, Water Res., 43 (2009) 2419–2430.
[15] H. Fu, X. Li, J. Wang, P. Lin, C. Chen, X. Zhang, I.M. Suffet, Activated carbon adsorption of quinolone antibiotics in water: performance, mechanism, and modeling, J. Environ. Sci., 56 (2017) 145–152.
[16] B. Kakavandi, A. Jonidi, R. Rezaei, S. Nasseri, A. Ameri, A. Esrafily, Synthesis and properties of Fe_3O_4-activated carbon magnetic nanoparticles for removal of aniline from aqueous solution: equilibrium, kinetic and thermodynamic studies, J. Environ. Health Sci. Eng., 10 (2013) 19.
[17] F. Liu, F. Niu, N. Peng, Y. Su, Y. Yang, Synthesis, characterization, and application of Fe_3O_4@SiO_2–NH_2 nanoparticles, RSC Adv., 5 (2015) 18128–18136.
[18] B. Kakavandi, A. Jonidi Jafari, R. Rezaei Kalantary, S. Nasseri, A. Esrafili, A. Gholizadeh, A. Azari, Simultaneous adsorption of lead and aniline onto magnetically recoverable carbon: optimization, modeling and mechanism, J. Chem. Technol. Biotechnol., 91 (2016) 3000–3010.
[19] M. Salari, M.H. Dehghani, A. Azari, M.D. Motevalli, A. Shabanloo, I. Ali, High performance removal of phenol from aqueous solution by magnetic chitosan based on response surface methodology and genetic algorithm, J. Mol. Liq., 285 (2019) 146–157.
[20] M. Farzadkia, E. Bazrafshan, A. Esrafili, J.-K. Yang, M. Shirzad-Siboni, Photocatalytic degradation of metronidazole with illuminated TiO_2 nanoparticles, J. Environ. Health Sci. Eng., 13 (2015) 35.
[21] B. Kakavandi, R. Rezaei Kalantary, A. Jonidi Jafari, A. Esrafily, A. Gholizadeh, A. Azari, Efficiency of powder activated carbon magnetized by Fe_3O_4 nanoparticles for amoxicillin removal from aqueous solutions: equilibrium and kinetic studies of adsorption process, J. Environ. Health Sci. Eng., 7 (2014) 21–34.
[22] Y. Tang, H. Guo, L. Xiao, S. Yu, N. Gao, Y. Wang, Synthesis of reduced graphene oxide/magnetite composites and investigation of their adsorption performance of fluoroquinolone antibiotics, Colloids Surf. A, 424 (2013) 74–80.
[23] Q. Song, Y. Fang, Z. Liu, L. Li, Y. Wang, J. Liang, Y. Huang, J. Lin, L. Hu, J. Zhang, C. Tang, The performance of porous hexagonal BN in high adsorption capacity towards antibiotics pollutants from aqueous solution, Chem. Eng. J., 325 (2017) 71–79.
[24] A. Mohseni-Bandpi, B. Kakavandi, R.R. Kalantary, A. Azari, A. Keramati, Development of a novel magnetite–chitosan

composite for the removal of fluoride from drinking water: adsorption modeling and optimization, RSC Adv., 5 (2015) 73279–73289.
[25] B. Kakavandi, A. Esrafili, A. Mohseni-Bandpi, A. Jonidi Jafari, R. Rezaei Kalantary, Magnetic Fe_3O_4@C nanoparticles as adsorbents for removal of amoxicillin from aqueous solution, Water Sci. Technol., 69 (2013) 147–155.
[26] M. Baziar, A. Azari, M. Karimaei, V.K. Gupta, S. Agarwal, K. Sharafi, M. Maroosi, N. Shariatifar, S. Dobaradaran, MWCNT-Fe_3O_4 as a superior adsorbent for microcystins LR removal: investigation on the magnetic adsorption separation, artificial neural network modeling, and genetic algorithm optimization, J. Mol. Liq., 241 (2017) 102–113.
[27] A. Sheikhmohammadi, M. Safari, A. Alinejad, A. Esrafili, H. Nourmoradi, E. Asgari, The synthesis and application of the Fe_3O_4@SiO_2 nanoparticles functionalized with 3-aminopropyltriethoxysilane as an efficient sorbent for the adsorption of ethylparaben from wastewater: synthesis, kinetic, thermodynamic and equilibrium studies, J. Environ. Chem. Eng., 7 (2019) 103315.
[28] A. Sheikhmohammadi, S.M. Mohseni, B. Hashemzadeh, E. Asgari, R. Sharafkhani, M. Sardar, M. Sarkhosh, M. Almasiane, Fabrication of magnetic graphene oxide nanocomposites functionalized with a novel chelating ligand for the removal of Cr (VI): modeling, optimization, and adsorption studies, Desal. Water Treat., 160 (2019) 297–307.
[29] C.A. Igwegbe, L. Mohmmadi, S. Ahmadi, A. Rahdar, D. Khadkhodaiy, R. Dehghani, S. Rahdar, Modeling of adsorption of Methylene Blue dye on Ho-$CaWO_4$ nanoparticles using response surface methodology (RSM) and artificial neural network (ANN) techniques, MethodsX, 6 (2019) 1779–1797.
[30] Y. Liu, X. Liu, W. Dong, L. Zhang, Q. Kong, W. Wang, Efficient adsorption of sulfamethazine onto modified activated carbon: a plausible adsorption mechanism, Sci. Rep., 7 (2017) 1–12.
[31] E. Çalışkan Salihi, S. Göktürk, Adsorption characteristics of sulfamethoxazole and metronidazole on activated carbon, Sep. Sci. Technol., 45 (2010) 244–255.
[32] I. Kariim, A.S. Abdulkareem, O.K. Abubakre, Development and characterization of MWCNTs from activated carbon as adsorbent for metronidazole and levofloxacin sorption from pharmaceutical wastewater: kinetics, isotherms and thermodynamic studies, Sci. Afr., 7 (2020) e00242.
[33] S. Manjunath, S.M. Kumar, H.H. Ngo, W. Guo, Metronidazole removal in powder-activated carbon and concrete-containing graphene adsorption systems: estimation of kinetic, equilibrium and thermodynamic parameters and optimization of adsorption by a central composite design, J. Environ. Sci. Health A, 52 (2017) 1269–1283.